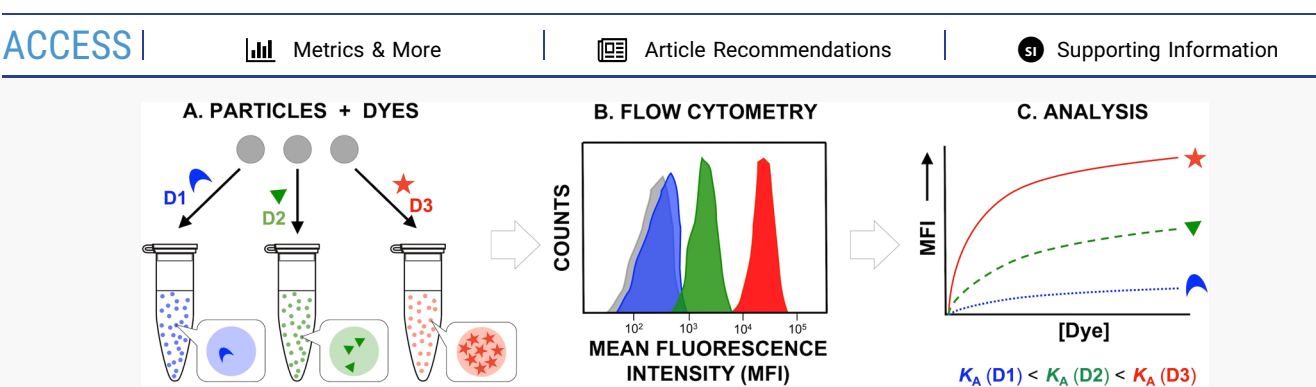
LANGMUIR

pubs.acs.org/Langmuir Article

Screening and Quantification of the Encapsulation of Dyes in Supramolecular Particles

Luis A. Prieto-Costas, Logan Milton, Carla M. Quiñones-Jurgensen, and José M. Rivera*





ABSTRACT: The encapsulation of therapeutic agents, such as drugs and vaccines, into colloidal particles offers an attractive strategy to enhance their efficacy. Previously, we reported the development of guanosine-based supramolecular colloidal particles suitable for encapsulating a broad array of guests ranging from small molecule drugs, like doxorubicin, to proteins, like GFP. Many biomedical applications of such particles require a precise determination of the amount of encapsulated therapeutic agents. Despite many studies describing the development of particle-based delivery systems, a general method for the precise and quick quantification of the encapsulated payload is still lacking. Here, we report a method based on flow cytometry measurements for complexes made from guanosine-based particles and a variety of commercially available fluorescent dyes. This method allows us to determine the apparent affinities of such dyes for two variants of these particles, which in turn provides insightful structure—affinity relationships. In contrast to the current methods, such as those that rely on fluorescence microscopy based on measurements of absorption/fluorescence of dissolved particles or on the supernatant of the solution, the reported method is suitable for high-throughput screening and more reproducible results. The protocol described here should be applicable to a wide variety of colloidal particles being developed around the world. Our group is currently expanding the scope to quantify the encapsulation of other molecules of biomedical interest, such as proteins and nucleic acids.

■ INTRODUCTION

The encapsulation of therapeutic agents, like drugs and vaccines, into colloidal particles offers an attractive strategy to enhance their efficacy. Examples include micelles, liposomes, 1,2 polymersomes, microbubbles, and inorganic-based particles. There is an increasing need to quantify the affinities of complex molecules in colloidal suspensions of macromolecules and nano/microparticles due to their increasing importance in drug delivery. More recent findings of the prevalence and importance of biological condensates also provide impetus to the development of versatile methods for the quantification of the partition of small molecules and macromolecules into colloidal particles.

Despite many studies describing the development of particle-based delivery systems, a general method for the precise and quick quantification of an encapsulated payload is still lacking. The main objectives of this study are (1) to develop an efficient method to quantify the complexation of small molecules to colloidal microparticles and (2) to apply the method to investigate the structure—property relationships

between the selected commercially available fluorescent dyes and supramolecular hacky sacks (SHS particles). The first objective stems from the fact that current methods have a low accuracy and/or low-throughput nature. The second will set the basis for developing the SHS particles for future applications in biomedicine, like affinity-based drug delivery and developing tools for cell biology studies.

We have reported the use of guanosine-based particles (e.g., SHS particles) as potential carriers for drug and vaccine delivery applications. For example, we reported the use of these particles for encapsulating the drug doxorubicin and various other molecules of biological interest, like proteins and

Received: August 3, 2021 Revised: September 19, 2021



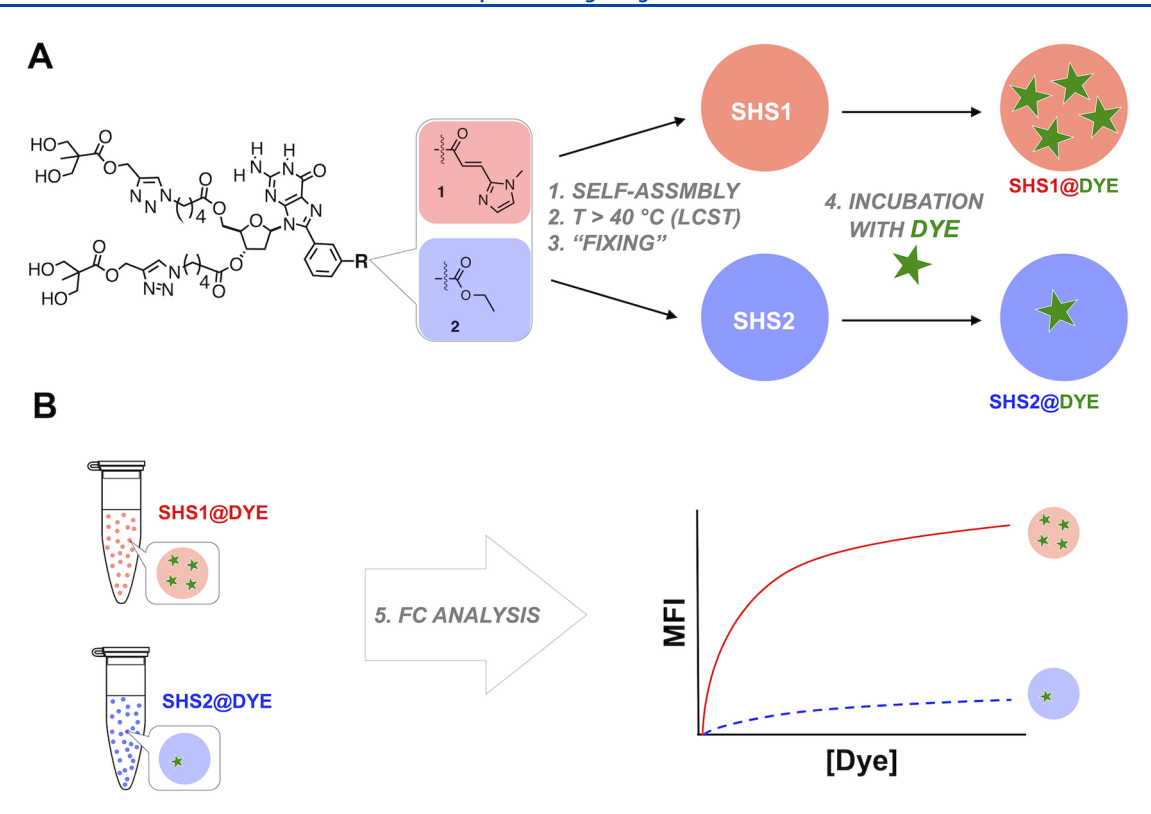


Figure 1. Experimental overview of the encapsulation methodology of dyes in SHS particles. (A) Guanosine monomers self-assembled in the presence of a cation to form SGQs. The self-assembled structures are further assembled by an increase in temperature to form SHS particles. The temperature of formation of SHS particles in this study is 40 °C. All experiments in this study were performed using "fixed" particles, meaning that they were kinetically stabilized by lowering the ionic strength of the solution to prevent their dissolution, which is prevented by abolishing the salting-in effect provided by the soft iodide anions. Dye incubation with SHS particles was carried out for 1 h at 40 °C. (B) After incubation, the SHS@Dye complexes were analyzed by FC, which enabled the construction of the saturation graphs used to calculate the apparent association constants.

DNA. 10,11 More recently, we demonstrated the use of SHS particles in improving the efficacy of DNA vaccines. 12

The move toward the application of the SHS particles prompted the need for precisely determining their affinity toward molecules of interest. However, most methods for quantifying loading, or determining encapsulation/complexation efficiency, rely on elaborate and time-consuming indirect or direct methods. Many of the indirect methods involve the dissolution of particles, often using organic solvents, followed by additional manipulations such as extraction, centrifugation, and filtration. These manipulations are then followed by quantification using a variety of methods including UV/vis spectroscopy, lad fluorescence spectrophotometry, spectroscopy, along others. Although the aforementioned methods provide flexibility, they suffer from slow throughput and relatively low accuracy.

Direct methods, in contrast, avoid some of the drawbacks of indirect methods, specifically those related to the introduction of measurement errors due to multiple physical manipulations. Thus, direct spectrophotometric or fluorometric methods offer advantages over indirect methods; however, colloidal particles at the higher end of the nanoscale and beyond are not amenable to standard procedures due to scattering interferences and sedimentation effects. Most direct methods rely on fluorescence microscopy techniques, like confocal laser scanning microscopy (CLSM), and the results are usually quantified using a parameter termed enrichment index (EI). 9,19 While the use of microscopy methods avoids the effort

involved in most indirect methods, they still suffer from their inherent low throughput and the potential artifacts introduced while assessing a relatively low number of particles. It is evident that there is a need to expand the repertoire of methods for direct quantification of particle loading and encapsulation efficiency.

Our group developed colloidal particles that serve as drug delivery agents. Guanosine-based particles, herein also referred to as SHS particles, are constructed from a hierarchical assembly of supramolecular G-quadruplexes (SGQs) after a change in their physical and/or chemical environment (e.g., increase in temperature and change in pH). These SGQs are in turn formed by the self-assembly of 2'-deoxyguanosine derivatives (G-monomers) in the presence of a templating salt (e.g., KI). We have evaluated the encapsulation of molecules by different qualitative methods like fluorescence microscopy but have yet to study the intrinsic affinities of these guests toward SHS particles. To achieve this, we have selected the flow cytometry (FC) technique, which is able to detect and measure the fluorescence of objects in the micrometer-size scale.

FC is a high-throughput technique that can detect individual cells and microparticles. In the study of colloidal particles, like multilamellar vesicles, ²² this technique is primarily used to determine the morphology and size. The technique can be used to study the affinity constant of molecules toward cell receptors, ^{23,24} the internalization of microparticles in cells, ²⁵ and the diffusion of small molecules in multilayer particles. ²⁶

Figure 2. Fluorescent dyes used in this study: resorufin (RE), methylene blue (MB), thioflavin T (ThT), malachite green (MG), fluorescein (F), 5(6)-carboxyfluorescein, mixed isomers (CF), rhodamine B (RB), 5(6)-carboxytetramethylrhodamine, mixed isomer (TA), thiazole orange (TO), ethidium bromide (EB), doxorubicin(DX), mesoporphyrin IX (MPIX), protoporphyrin IX (PIX), and TmPyP4 (TM).

There are, however, relatively few studies of FC used for the measurement of affinity constants of particles. ^{27,28} Temmerman and co-workers studied the affinity of fluorescent proteins with membrane lipids, ²⁷ while Liu and co-workers ²⁸ measured biomacromolecule binding in modified polystyrene microbeads; however, to the best of our knowledge, there are no studies of the use of FC to measure the affinity constants of colloidal particles toward fluorescent dyes.

Here, we report a method based on FC measurements of samples made from complexes of SHS particles with a variety of fluorescent dyes. The method allows us to determine the apparent affinities of such dyes for two variants of the particles, which in turn provides insightful structural—affinity relationships (Figure 1B). These findings suggest that relatively weak, but specific, interactions are at play between the dyes and the constituents of the SHS particles. Our method provides quick and reproducible data in a nondestructive fashion, which represents an advantage over other direct methods, like those based on measurements of the absorption/fluorescence of dissolved particles or of the supernatant of the solution.

■ EXPERIMENTAL SECTION

Materials. All commercially available reagents were used without further purification. 5(6)-Carboxyfluorescein mixed isomers were purchased from AnaSpec Inc. (5 and 6)-Carboxytetramethylrhodamine mixed isomers were purchased from Biosearch Technologies. All other dyes were purchased from Sigma-Aldrich. G-derivatives 1 and 2 were synthesized following the procedures published elsewhere. 20,21

Dynamic Light Scattering (DLS) and Zeta Potential. A Zetasizer Nano ZS (model ZEN 3600) from Malvern with a 4 mW laser of 632.8 nm wavelength and a backscatter angle of 173° was used to measure the hydrodynamic diameter, zeta potential, and polydispersity index of the **SHS1** and **SHS2** particles at 25 °C. All the measurements were performed following the incubation

procedure (see Supporting Information). The instrument data were exported using the Malvern Zetasizer Software (v. 7.10) and imported into Microsoft Excel to construct the DLS plots.

Flow Cytometry. FC measurements were conducted using a BD Accuri C6 flow cytometer from BD Biosciences with a standard laser configuration (488 and 640 nm) and detectors (FL1 525/25, FL2 585/15, FL3 670 LP, and FL4 675/25). Eppendorf tubes containing the SHS@Dye samples were vortexed before they were introduced to the sample injector port of the flow cytometer. This process was repeated with each dye concentration (0, 0.1, 1, 3, 6, 12, 24, and 48 μ M). The concentrations used for **RB**, **MG**, and **TO** were 0, 0.1, 1, 3, 6, 12, and 24 μ M. All other dyes used 0, 1, 3, 6, 12, 24, and 48 μ M concentrations. For each dye, a forward scatter versus side scatter density plot (FSC vs SSC) was used to create a gate for the SHS control. This gate was used for every concentration. At least 10 K events were recorded for each experiment. Histograms were generated from each gated density plot. The change in the median fluorescence intensity of each sample was plotted as a function of the concentration to generate saturation binding curves. All SHS@Dye complexes were excited with a 488 nm laser except SHS@MG and SHS@MB for which 640 nm was used instead. The fluorescence in detector FL1 was used for F, CF, TO, and ThT; FL2 was used for RB, DX, RE, and TA; FL3 was used for EB, TM, PIX, and MPIX; and FL4 was used for MG and MB.

Confocal Laser Scanning Microscopy. Confocal microscopy images were obtained using a Nikon Eclipse Ti-E inverted microscope with an emission range of 400–730 nm. The objective used for all the samples was a Plan Apo alpha 100X with oil. Rhodamine B, TAMRA, and resorufin were excited with a 561 nm laser. Fluorescein, carboxy fluorescein, ethidium bromide, TmPyP4, protoporphyrin IX, mesoporphyrin IX, doxorubicin, thiazole orange, and thioflavin T were excited with a 488 nm laser. Malachite green and methylene blue were excited at 640 nm. Other parameters, such as laser power and HV, are reported in the Supporting Information (Table S3) for dyes used in EI experiments. After the incubation process, 10 μL of SHS@Dyes from each sample was added to the microscope slide and covered with a glass cover slip. Images were taken 1 day after preparing the slides.

Data Analysis and Calculations. The average and standard deviation of the median fluorescence intensity (MFI) data were calculated from three measurements. The apparent dissociation constant (K_D) was obtained using GraphPad Prism version 6.00 for Mac OS X, GraphPad Software, La Jolla California USA, www. graphpad.com. K_D values were determined using a hyperbolic curve fitting or a one-site specific binding equation $(y = B_{\text{max}} \times X / (K_D + X))$. $K_{\rm D}$ is defined as the concentration of dye needed to achieve halfmaximum binding at equilibrium. The association constant (K_A) was calculated as the reciprocal of K_D . Data points were removed from the saturation graphs when the coefficient of determination (R2) of the curve fitting was below 0.9. Points that did not visually follow the expected hyperbolic curve fitting were systematically removed until R2 was above 0.9. For the EI studies, the average and standard deviation represent the ratio of the fluorescence inside and outside of at least three SHS particles.

■ RESULTS AND DISCUSSION

Guanosine-based colloidal particles can be analyzed by FC due to their size ($\sim 1~\mu m$). The monomer unit used in the formation of the particles affects the emerging properties at the microscale. Previously, we discovered that precise modifications in the G-derivatives control the temperature of formation of the colloidal particles. Also, the incorporation of a pH-sensitive moiety, like an imidazole, to the monomer controls the formation of SHS particles via changes in pH. Since changes in the constituent G-derivatives lead to different macroscopic properties, we selected two G-derivatives to test the affinity of targeted molecules toward the resulting SHS particles.

The SHS particles in this study were prepared from either one of the G-derivatives 1 and 2, which differ in the group attached to the *meta*-carbonyl phenyl ring joined to the C8 position of the guanine moiety. Derivative 1 has a conjugated imidazole group, while 2 contains an ethyl ester (Figure 1). Both compounds self-assemble to SGQs and SHS particles in phosphate-buffered saline (PBS) containing 2 M KI. Subsequent reduction of the ionic strength kinetically stabilizes (or "fixes)" the SHS particles, which are then suitable for the encapsulation of a wide variety of guests like dyes and proteins. For this study, kinetically stabilized SHS particles made from 1 and 2 will be termed SHS1 and SHS2, respectively.

At the microscale, the differences between these particles are the size (i.e., hydrodynamic diameter) and Z-potential (i.e., surface charge of the particle³⁰). The size of the particles is 2 and 1.3 μ m for SHS1 and SHS2 at 25 °C, respectively (Figure S1 and Table S1). The Z-potential is -16 mV and -11 mV for SHS1 and SHS2 at 25 °C, respectively (Figure S1 and Table S1). For both SHS1 and SHS2, parameters like monomer and salt concentrations, pH, temperature, and incubation time were kept identical to minimize undesired variability that may complicate data analysis.

We selected 14 commercially available dyes (Figure 2) previously reported to interact with DNA-quadruplexes (G4 DNA), such as porphyrins (e.g., TmPyP4),³¹ or guanosine-based colloidal particles, such as xanthene dyes (e.g., rhodamine B).¹¹ Earlier, we had established that the SHS particles are made from SGQs; thus, we hypothesized that many interactions with the selected guests would be similar to nucleic acid-based G-quadruplexes (e.g., G4-DNA/RNA). Both G4-DNA/RNA and SGQs have planar aromatic regions on their surfaces that serve as potential binding sites for aromatic molecules through end-stacking interactions (e.g., $\pi-\pi$ interactions). The selected cationic and anionic

porphyrins (TM, PIX, and MPIX) have analogous planar binding surfaces that complement the G4 structure. ^{32,33} Other smaller aromatic dyes bind to these structures via end-stacking, but we must also consider the ionic charge of these dyes (positive, negative, or zwitterionic). One of the binding modes of G4-DNA is the electrostatic interactions of the negative phosphate backbone with positive molecules, like the tetracationic TmPyP4. Although the SGQs have no phosphate backbone, the negative zeta potential of the resulting SHS particles may lead to a preference for cationic molecules.

Previously, we reported that the main encapsulation mechanism was physical absorption (i.e., diffusion) of dyes inside SHS particles.¹¹ Consequently, the affinity of a dye toward the SHS particles should be affected by physicochemical characteristics, such as aromatic area, ionic charge, and size. We hypothesized that the main differences in affinity of these dyes toward SHS particles are determined by both the structural modifications of the G-derivatives and the resulting properties of the assembly (e.g., size and Z-potential) at the mesoscopic level. Given this, we will use molecular descriptors to correlate the characteristics of the molecules that affect the resulting affinities toward the SHS particles.

FC Studies. The method to determine the affinity of dyes toward SHS particles consists of mixing different concentrations of dyes with SHS particles to form a complex (SHS#@ Dye, where # is the identifier of the constituent G-derivative used to form the SHS particle) and using FC to measure their MFI as a function of dye concentration. Depending on the type of dye in the colloidal complex, we selected the 488 or 640 nm excitation laser in the instrument. Figure 3 shows the encapsulation of RB in SHS1 (SHS1@RB) and SHS2 (SHS2@RB), specifically, the forward scatter (FSC) versus side scatter (SSC) FC density plots as well as histograms of SHS1. FSC provides information regarding the size of the objects or events, while SSC gives insights into the changes in the internal structure, also called granularity. 34 Events recorded (at least 10 K) shown in density plots and gated histograms are of SHS1 before and after encapsulation of RB. Histograms generated from the density plots show how the fluorescent particle population changes as a function of dye concentration. A shift in the histogram before and after the encapsulation is indicative of the formation of the SHS@RB complex. The fluorescence of the SHS@RB complex increases proportionally with the RB encapsulation concentration until equilibrium or saturation is achieved. The MFI recorded was plotted as a function of dye concentration to construct saturation plots, which are used to calculate the dissociation constant using PRISM GraphPad (see Supporting Information for details).

Density Plots and Histograms of the SHS@Dye Complexes. The density plots of SHS@RB complexes suggest that the internal structure does not change by the encapsulation of the dye, which is similar to the results for most other SHS complexes (Figure 3). This may be due to the favorable π - π interactions of dyes with the aromatic surface of the SGQs that make up the SHS particle. However, there are density plots from other complexes that show interesting deviations from this behavior.

For example, density plots of SHS complexes constructed from PIX and MPIX suggest changes in the internal structure, which we hypothesized were due to dye aggregation.³⁵ Control measurements recorded after 1 min indicate aggregation of dyes MPIX and PIX without SHS particles, which in turn suggests that the density plots of SHS@MPIX or SHS@PIX

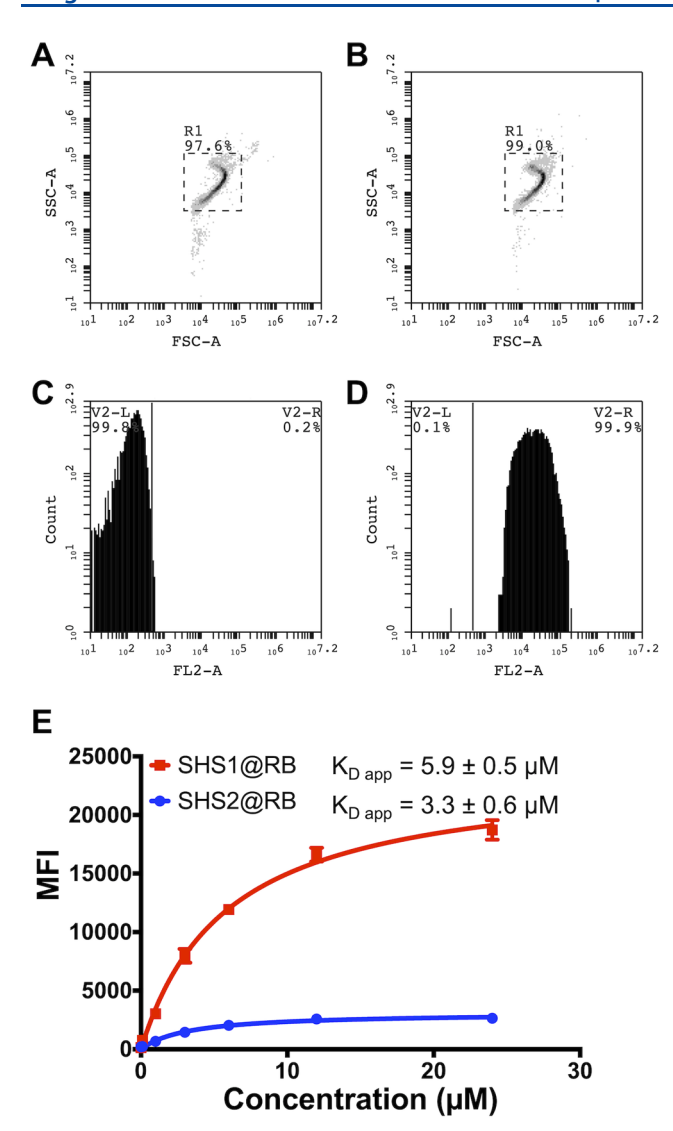


Figure 3. FC data and saturation binding curves for the encapsulation of RB in SHS particles. (A, B) FSC versus SSC density plots of the encapsulation of RB in SHS1 and (C, D) the corresponding histograms generated from gated density plots. Concentration of the dye: (A, C) 0 μ M and (B, D) 24 μ M. The histograms were generated from a gated density plot with at least 10 K events recorded. The vertical line of the histograms indicates the boundary of the autofluorescence of the SHS particle. Events to the right of the line represent an increase in fluorescence due to the encapsulation of RB. Excitation laser: 488 nm and emission channel: FL2 or 585 nm. (E) Saturation binding curves of the encapsulation of RB in SHS1 (red) and SHS2 (blue). MFI was plotted as a function of encapsulation concentrations (0, 0.1, 1, 3, 6, 12, and 24 μ M). K_D was calculated via curve fitting with PRISM GraphPad 6 as described in the general Experimental Section and was subsequently used to calculate the corresponding K_A values $(1/K_D)$. All measurements were carried out in triplicate and after 1 h at 40 °C. Error bars represent the average of three measurements. SHS1 and SHS2: 299 μM Gderivative, 121 mM KI, PBS, pH 7.4.

show a mixture of dye aggregation and SHS complex that will affect the affinity measurements.³⁴ In contrast, while the density plots of SHS@TO show patterns that also suggest changes to the internal structure (e.g., supramolecular arrangements) of the SHS particles (Figure S2), the possibility that this behavior was due to dye aggregation was discarded

given the lack of evidence gathered from control measurements (Figure S2). We expect that future studies using other techniques, like Raman spectroscopy, may help us obtain more details about this phenomenon.

Saturation Plots from FC Studies. The saturation binding curves in Figure 4 show fluorescence intensity as a

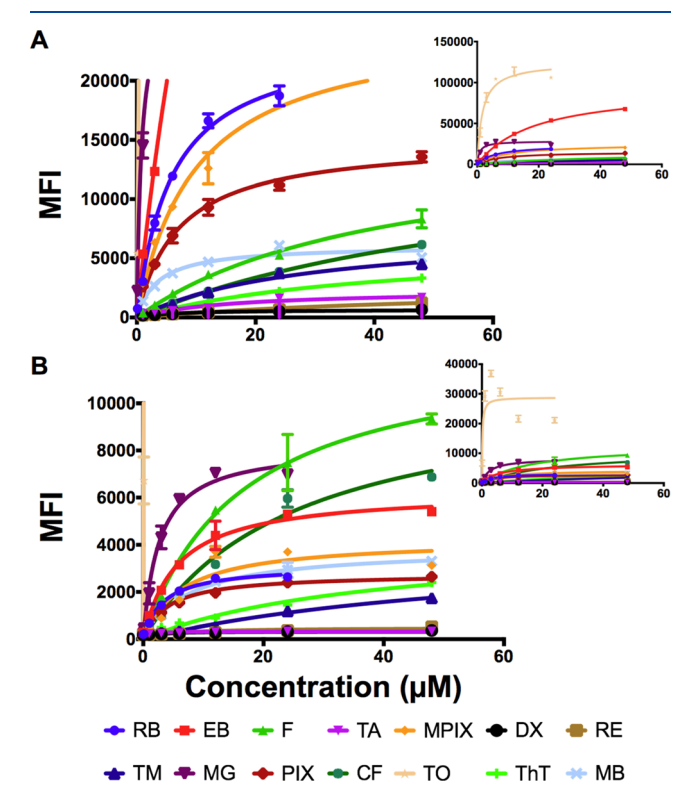


Figure 4. Saturation binding curves for the encapsulation of fluorescent dyes in (A) SHS1 and (B) SHS2. MFI was plotted as a function of concentration of the encapsulated dye. Error bars represent the standard deviation of the average of triplicate measurements. SHS: 299 μ M 1, 121 mM KI, PBS, pH 7.4. The inset on the upper right corners shows a zoom out image of the saturation binding curves for the maximum MFI of (A) 150 K and (B) 40 K.

function of the concentration of the SHS@Dye complexes after FC measurements. Previously, we observed that the encapsulation of **RB** in **SHS1** results in a higher MFI compared to that in **SHS2**. The binding curves show different MFI maxima or saturation points that are determined by the quantum yield of the dyes, the excitation maximum, or the intrinsic affinity. Here, we can see that most of the complexes of **SHS1** have higher MFI than **SHS2**, which might be due to the differences in the size of these particles. These graphs were used to calculate the corresponding apparent K_A for the SHS complexes.

Apparent Association Constants. The graphs shown in Figure 5 show the results of K_A generated from the saturation graphs of SHS@Dye complexes. If all the dyes tested had equal quantum yields, a higher MFI at a given concentration would imply a higher affinity. Since this is not the case, a simple visual assessment of the saturation does not allow a direct comparison between dyes. The shape of the curve, however, like those of dyes leading to steep initial binding curves at low concentrations results in high affinity constants (e.g., MG).

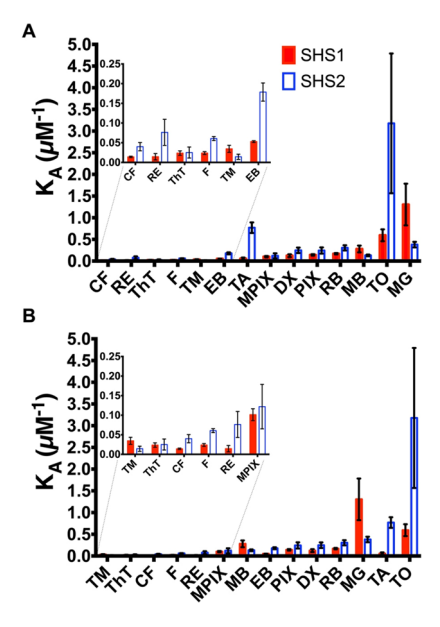


Figure 5. Apparent K_A values of fluorescent dyes toward SHS1 and SHS2 determined from FC measurements. K_A values are arranged in ascending order for (A) SHS1 and (B) SHS2. Error bars represent the standard error of the measurement reported by PRISM GraphPad. The insets highlight the six dyes with the lowest K_A values for each SHS.

Evaluation of the overall data reveals that cationic dyes such as **TO** and **MG** have good affinities toward SHS particles as well as zwitterionic dyes like **RB** and **TA**. The dyes **TO** and **MG** are known to interact with G4-DNA^{36,37} and other synthetic G-quadruplexes.³⁸ In order to unveil the potential relationships between dyes and their affinities toward the SHS particles, we constructed correlation graphs of K_A as a function of various molecular descriptors for the dyes (Figures S5–S7).

Molecular descriptors, such as lipophilicity (log P), molecular weight (MW), the expected charge of the dye at pH 7.4, and the accessible surface area (ASA), were plotted as a function of K_A . While these plots revealed small correlations, some interesting trends surfaced. For example, for SHS1, the log P value shows a minor increase in affinity as a function of K_A , while for SHS2, it shows a slight decrease instead. This may be because the SHS1 particle is more hydrophobic and thus attracts lipophilic compounds. The larger and more lipophilic nature of the vinyl imidazole moiety attached to the meta-carbonyl group in 1 makes the corresponding assemblies more hydrophobic than those of 2, which instead has an ethoxy moiety. This is consistent with previous studies by us,³⁹ specifically the fact that a higher amount of salt needed to dissolve the G-derivative 1 via a "salting-in" process for selfassembly and a decrease in the lower critical solution temperature promote the formation of the SHS particles. Nevertheless, the fact that the difference in slope is small suggests that lipophilicity, as described by the log P values, is only a minor contributor determining the native affinity toward SHS particles.

Other correlations using the descriptors of MW and ASA show a slight decrease in affinity as a function of size (Figure S6). This is consistent with studies from our group showing that molecules with a large molecular mass do not diffuse completely within an SHS particle, which in turn is indicative of low affinities.¹¹

There is a weak correlation between the affinity of the dyes and their overall charge. The Davis group reported the use of an anionic microgel made from G4-quartets that bind cationic dyes due to the structural properties of G4 (planar conformation) and complementary charges. They showed that cationic dyes such as ThT, TO, MB, and a derivative of MG (crystal violet) stabilize the gel, while RB, a nonplanar zwitterionic dye, shows weak interactions. In our case, both kinds of particles increase the affinity with cationic molecules. Similarly, the enhanced affinity of cationic or zwitterionic dyes toward the negatively charged SHS particles is consistent with these observations.

The molecular descriptors of the dyes reveal structural—affinity correlations for their affinity toward SHS particles. To further understand these trends, the affinities were analyzed based on their charge and their broad classification as derivatives of xanthene or porphyrins (Figure S8).

The anionic xanthene dyes F and CF show low affinity toward both SHS particles tested, which is consistent with repulsive interactions due to the negative Z-potential of the particles. In contrast, the zwitterionic dyes RB and TA show moderate affinity. The highest affinities for SHS1 among the xanthene dyes were found for RB and MB, which is interesting considering that the former is neutral (zwitterionic) while the latter is cationic. In contrast, for SHS2, the dye TA shows not just the highest affinity but also the largest difference in affinity relative to SHS1. These results underscore that for the xanthene family, the overall molecular charge is a key parameter determining their affinity toward the SHS particles.

Among the three porphyrins evaluated, TM showed around an order of magnitude lower affinity than the closely related PIX and MPIX, which in turn show very similar affinities between them. This was anticipated given that what differentiates these molecules is just an unsaturated ethyl group. Relative to PIX and MPIX, the porphyrin TM shows lower affinity toward SHS1 but not toward SHS2. In general, porphyrins show a propensity for binding via end-stacking to a wide variety of G4-DNA/RNA. 31,40,41 In the case of TM, however, this binding mode is dampened due to the steric hindrance imposed by the perpendicular arrangement of the pyridinium groups as reported in the literature⁴² and corroborated by molecular modeling studies (Figure S58). We hypothesize that these steric effects are also responsible for the apparent poor affinity of **TM** toward the constituent SGQs. Although in general cationic molecules show higher affinities toward these systems, the low affinity of TM relative to PIX and MPIX underscores the importance of other parameters. Moreover, despite PIX and MPIX having higher affinities than TM, their affinities are not significantly higher than those of the other anionic dyes and are generally weaker than those of cationic dyes. Within the set of dyes tested, there are no strong trends when evaluating the affinities of cationic dyes.

Confocal Microscopy Studies. A CLSM provides high-resolution images of cells and microparticles in two different modes: (1) differential interference contrast and (2) fluorescence. Previously, we have used this technique to visualize the encapsulation of selected compounds in qualitative measurements. In the most basic application of CLSM, images of particles complementing the FC technique are used to confirm the encapsulation of a target compound. However, Schuster et al. Preported the use of EI determined by CLSM in order to quantify the efficiency of encapsulation inside liquid particles. The EI provides an alternative

measurement of the partition of dyes inside and outside a colloidal particle. With this precedent from the literature in mind, we performed CSLM measurements to complement the affinity studies by FC and gather additional quantitative data.

The images obtained from CLSM measurements are consistent with the FC results showing that, except for CF, all other dyes partition preferentially within (i.e., are enriched) the SHS particles (Figure 6). Even at higher concentrations (12 μ M), CF is excluded from the SHS particles, which agrees well with the apparent low affinity determined by the FC method. The resulting EI for the SHS@Dye complexes showed that in most cases, for most of the dyes tested, the enrichment

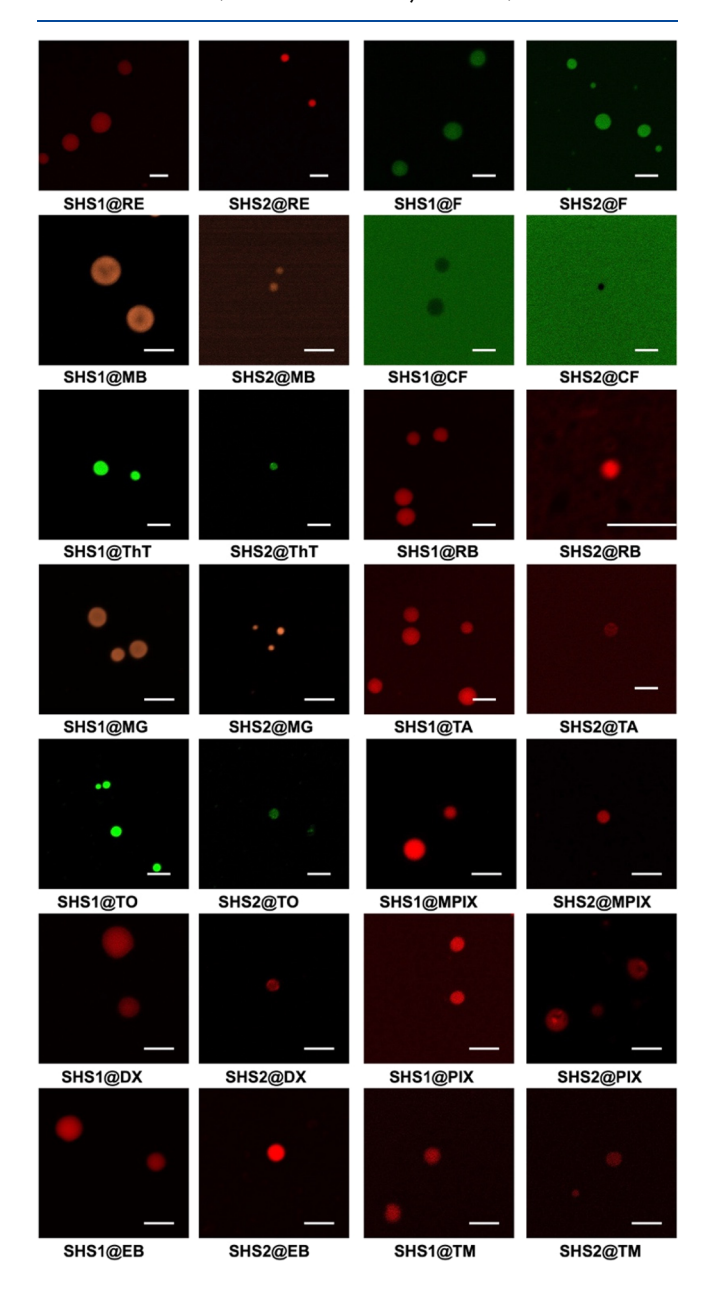


Figure 6. Confocal microscopy images for the **SHS1** and **SHS2** particles incubated with fluorescent dyes. All dyes were used at a concentration of 3 μ M except for CF (12 μ M). The laser used for F, CF, MPIX, PIX, TM, EB, ThT, TO, and DX was 488 nm, and for RB, TA, RE, it was 561 nm, and for MG and MB, it was 640 nm. **SHS1** and **SHS2**: 299 μ M G-derivative, 121 mM KI, PBS, pH 7.4. All scale bars are 5 μ m.

is higher in the larger SHS1 particles relative to the smaller SHS2 particles (Figure 7), which likely reflect the smaller volume for the latter.

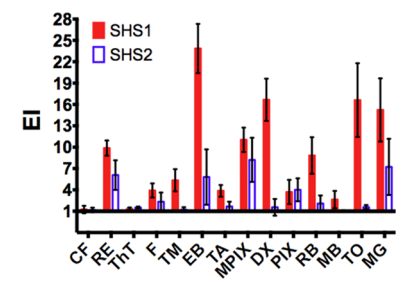


Figure 7. Confocal microscopy reveals distinct quantitative information about the binding of fluorescent dyes toward SHS particles. The bar graph of the EI of dyes in **SHS1** and **SHS2** determined by confocal microscopy data. EI was calculated as the ratio of the fluorescence inside and outside of the SHS particle. The dye concentration used for the EI experiments was 3 μ M. Error bars represent the average of at least three SHS particles. **SHS1** and **SHS2** concentrations are 299 μ M G-derivative, 121 mM KI, PBS, pH 7.4. All samples were incubated for 1 h with or without dye. **RB**, **TA**, and **RE** were excited using a 561 nm laser. **F**, **DX**, **EB**, **TM**, **PIX**, **MPIX**, **ThT**, and **TO** were excited using a 488 nm laser. **MG** and **MB** were excited with the 640 nm laser. For further details, see the Supporting Information.

The CLSM images also reveal differences in the distribution of dyes within the particles. In particular, cationic dyes MB and MG appear to concentrate on the periphery of the SHS1 particles, which we hypothesize might be due to an interfacial aggregation/crystallization process. Further studies using a larger set of dyes and alternative spectroscopic techniques will be required to obtain more details about this phenomenon.

Both FC and CLSM are single-particle detection techniques that complement each other, but in general, the former has multiple advantages over the latter. The FC technique can differentiate between an encapsulated dye and no dye, while CLSM is not sensitive enough to make these distinctions with some dyes (e.g., PIX) as demonstrated by control measurements shown in Figure S9. Also, the affinity constants calculated from FC studies appear to be unaffected by the differences in the size of the particles studied. In contrast, the EI shows a direct correlation between high enrichment and size. This disadvantage is compounded by the fact that the EI is calculated from a relatively small number of measurements. While increasing the number of particles considered in the calculations of EI is possible, time and other technical constraints (e.g., photobleaching) make it impractical to obtain more than a small percentage of thousands of events measured via FC. The FC method also allows us to compare between dyes in a high-throughput manner, while confocal microscopy has certain parameters and adjustments per dye that make the measurements more time consuming.4

CONCLUSIONS

We described a method to determine the affinity constants of dyes toward SHS particles using FC and analyzed the results with the help of molecular descriptors. We observed that small modifications in the G-derivatives slightly affect the affinity of the dyes depending on the hydrophobicity or lipophilicity of the fluorescent molecules. In general, cationic, small molecules, like **MG** and **TO**, show good affinity toward the SHS particles

likely due to their electrostatic attraction and negative Z-potential. Nevertheless, changing the size of a SHS particle can affect the loading capacity for a specific dye but not necessarily its affinity. We also showed that confocal microscopy studies confirm the selective partition of most dyes from the bulk solution within the SHS particles.

We are currently applying this method for the evaluation of the affinity of proteins toward SHS particles. We are also evaluating the formation SHS particles made with Gderivatives modified with affinity ligands to enhance and modulate the corresponding native affinities. Results for such studies will be reported soon.

ASSOCIATED CONTENT

Supporting Information

The Supporting Information is available free of charge at https://pubs.acs.org/doi/10.1021/acs.langmuir.1c02065.

Preparative protocols, DLS and Z-potential data, FC data, histograms and density plots, saturation curves, CLSM images, and molecular models (PDF)

AUTHOR INFORMATION

Corresponding Author

José M. Rivera — Department of Chemistry and Molecular Sciences Research Center, University of Puerto Rico at Río Piedras, San Juan, Puerto Rico 00926, United States; orcid.org/0000-0001-7089-7640;

Email: jose.rivera151@upr.edu

Authors

Luis A. Prieto-Costas – Department of Chemistry and Molecular Sciences Research Center, University of Puerto Rico at Río Piedras, San Juan, Puerto Rico 00926, United States

Logan Milton – Department of Chemistry and Molecular Sciences Research Center, University of Puerto Rico at Río Piedras, San Juan, Puerto Rico 00926, United States

Carla M. Quiñones-Jurgensen — Department of Chemistry and Molecular Sciences Research Center, University of Puerto Rico at Río Piedras, San Juan, Puerto Rico 00926, United States

Complete contact information is available at: https://pubs.acs.org/10.1021/acs.langmuir.1c02065

Notes

The authors declare no competing financial interest.

ACKNOWLEDGMENTS

We thank Dr. Valance Washington for lending us the flow cytometer used in this study. We also thank the Neuroimaging and Electrophysiology Facility (Grant NIH-NIGMS P20GM103642) and Bismark A. Madera Soto, MS, MT, MLS (ASCP) CM for the CLSM experiments and the Molecular Sciences Research Center. We are also grateful to the NSF REU (Grant 1757365) and the RISE (Grant SR25GM061151) Programs for financial support to L.J.M. and L.A.P.-C., respectively.

■ REFERENCES

(1) Kraft, J. C.; Freeling, J. P.; Wang, Z.; Ho, R. J. Y. Emerging Research and Clinical Development Trends of Liposome and Lipid Nanoparticle Drug Delivery Systems. *J. Pharm. Sci.* **2014**, *103*, 29–52.

- (2) Heyes, J.; Palmer, L.; Bremner, K.; MacLachlan, I. Cationic Lipid Saturation Influences Intracellular Delivery of Encapsulated Nucleic Acids. *J. Controlled Release* **2005**, *107*, 276–287.
- (3) Burke, P. A.; Pun, S. H.; Reineke, T. M. Advancing Polymeric Delivery Systems Amidst a Nucleic Acid Therapy Renaissance. *ACS Macro Lett.* **2013**, *2*, 928–934.
- (4) Lee, L.; Cavalieri, F.; Ashokkumar, M. Exploring New Applications of Lysozyme-Shelled Microbubbles. *Langmuir* **2019**, 35, 9997–10006.
- (5) Kundu, S.; Ghosh, M.; Sarkar, N. State of the Art and Perspectives on the Biofunctionalization of Fluorescent Metal Nanoclusters and Carbon Quantum Dots for Targeted Imaging and Drug Delivery. *Langmuir* **2021**, *37*, 9281–9301.
- (6) Canton, I.; Battaglia, G. Endocytosis at the Nanoscale. Chem. Soc. Rev. 2012, 41, 2718–2739.
- (7) Biswas, A.; Shukla, A.; Maiti, P. Biomaterials for Interfacing Cell Imaging and Drug Delivery: An Overview. *Langmuir* **2019**, *35*, 12285–12305.
- (8) Karg, M.; Pich, A.; Hellweg, T.; Hoare, T.; Lyon, L. A.; Crassous, J. J.; Suzuki, D.; Gumerov, R. A.; Schneider, S.; Potemkin, I. I.; Richtering, W. Nanogels and Microgels: From Model Colloids to Applications, Recent Developments, and Future Trends. *Langmuir* **2019**, 35, 6231–6255.
- (9) Schuster, B. S.; Reed, E. H.; Parthasarathy, R.; Jahnke, C. N.; Caldwell, R. M.; Bermudez, J. G.; Ramage, H.; Good, M. C.; Hammer, D. A. Controllable Protein Phase Separation and Modular Recruitment to Form Responsive Membraneless Organelles. *Nat. Commun.* 2018, 9, 2985.
- (10) Betancourt, J. E.; Subramani, C.; Serrano-Velez, J. L.; Rosa-Molinar, E.; Rotello, V. M.; Rivera, J. M. Drug Encapsulation within Self-Assembled Microglobules Formed by Thermoresponsive Supramolecules. *Chem. Commun.* **2010**, *46*, 8537.
- (11) Negrón, L. M.; Díaz, T. L.; Ortiz-Quiles, E. O.; Dieppa-Matos, D.; Madera-Soto, B.; Rivera, J. M. Organic Nanoflowers from a Wide Variety of Molecules Templated by a Hierarchical Supramolecular Scaffold. *Langmuir* **2016**, *32*, 2283–2290.
- (12) Santos, S.; Ramírez, M.; Miranda, E.; Reyes, N.; Martínez, O.; Acosta-Santiago, M.; Rivera, J. M.; Otero, M. Enhancement of Immune Responses by Guanosine-Based Particles in DNA Plasmid Formulations against Infectious Diseases. *J. Immunol. Res.* **2019**, 2019, No. 2400371
- (13) Mason, A. F.; Buddingh', B. C.; Williams, D. S.; van Hest, J. C. M. Hierarchical Self-Assembly of a Copolymer-Stabilized Coacervate Protocell. *J. Am. Chem. Soc.* **2017**, *139*, 17309–17312.
- (14) Wu, H.; Zhu, L.; Torchilin, V. P. PH-Sensitive Poly(Histidine)-PEG/DSPE-PEG Co-Polymer Micelles for Cytosolic Drug Delivery. *Biomaterials* **2013**, *34*, 1213–1222.
- (15) Broaders, K. E.; Cohen, J. A.; Beaudette, T. T.; Bachelder, E. M.; Frechet, J. M. J. Acetalated Dextran Is a Chemically and Biologically Tunable Material for Particulate Immunotherapy. *Proc. Natl. Acad. Sci.* **2009**, *106*, 5497–5502.
- (16) Wu, D.; Wang, C.; Yang, J.; Wang, H.; Han, H.; Zhang, A.; Yang, Y.; Li, Q. Improving the Intracellular Drug Concentration in Lung Cancer Treatment through the Codelivery of Doxorubicin and MiR-519c Mediated by Porous PLGA Microparticle. *Mol. Pharmaceutics* **2016**, *13*, 3925–3933.
- (17) Kim, S.-H.; Kim, J. W.; Kim, D.-H.; Han, S.-H.; Weitz, D. A. Polymersomes Containing a Hydrogel Network for High Stability and Controlled Release. *Small* **2013**, *9*, 124–131.
- (18) Wang, L.; Chierico, L.; Little, D.; Patikarnmonthon, N.; Yang, Z.; Azzouz, M.; Madsen, J.; Armes, S. P.; Battaglia, G. Encapsulation of Biomacromolecules within Polymersomes by Electroporation. *Angew. Chem., Int. Ed.* **2012**, *51*, 11122–11125.
- (19) Klein, I. A.; Boija, A.; Afeyan, L. K.; Hawken, S. W.; Fan, M.; Dall'Agnese, A.; Oksuz, O.; Henninger, J. E.; Shrinivas, K.; Sabari, B. R.; Sagi, I.; Clark, V. E.; Platt, J. M.; Kar, M.; McCall, P. M.; Zamudio, A. V.; Manteiga, J. C.; Coffey, E. L.; Li, C. H.; Hannett, N. M.; Guo, Y. E.; Decker, T.-M.; Lee, T. I.; Zhang, T.; Weng, J.-K.; Taatjes, D. J.; Chakraborty, A.; Sharp, P. A.; Chang, Y. T.; Hyman, A. A.; Gray, N.

- S.; Young, R. A. Partitioning of Cancer Therapeutics in Nuclear Condensates. *Science* **2020**, *368*, 1386–1392.
- (20) Betancourt, J. E.; Rivera, J. M. Nonpolymeric Thermosensitive Supramolecules. *J. Am. Chem. Soc.* **2009**, *131*, 16666–16668.
- (21) Negrón, L. M.; Meléndez-Contés, Y.; Rivera, J. M. Patchy Supramolecules as Versatile Tools To Probe Hydrophobicity in Nanoglobular Systems. *J. Am. Chem. Soc.* **2013**, *135*, 3815–3817.
- (22) Hema Sagar, G.; Tiwari, M. D.; Bellare, J. R. Flow Cytometry As a Novel Tool to Evaluate and Separate Vesicles Using Characteristic Scatter Signatures. *J. Phys. Chem. B* **2010**, *114*, 10010–10016.
- (23) Keller, M.; Mahuroof, S. A.; Hong Yee, V.; Carpenter, J.; Schindler, L.; Littmann, T.; Pegoli, A.; Hübner, H.; Bernhardt, G.; Gmeiner, P.; Holliday, N. D. Fluorescence Labeling of Neurotensin (8–13) via Arginine Residues Gives Molecular Tools with High Receptor Affinity. ACS Med. Chem. Lett. 2020, 11, 16–22.
- (24) Stein, R. A.; Wilkinson, J. C.; Guyer, C. A.; Staros, J. V. An Analytical Approach to the Measurement of Equilibrium Binding Constants: Application to EGF Binding to EGF Receptors in Intact Cells Measured by Flow Cytometry †. *Biochemistry* **2001**, *40*, 6142–6154
- (25) Semmling, M.; Kreft, O.; Muñoz Javier, A.; Sukhorukov, G. B.; Käs, J.; Parak, W. J. A Novel Flow-Cytometry-Based Assay for Cellular Uptake Studies of Polyelectrolyte Microcapsules. *Small* **2008**, *4*, 1763–1768.
- (26) Vardanyan, I.; Navoyan, Z.; Moya, S. E.; Arakelyan, V.; Donath, E. Flow Cytometry Study of the Non-Fickean Diffusion of Small-Charged Molecules in Poly(Diallyl Dimethyl Ammonium Chloride)/Poly(Styrene Sodium Sulfonate) Multilayers: Impact of the Layer Number, Top Layer, and Concentration of Diffusing Molecules. J. Phys. Chem. B 2019, 123, 2182–2189.
- (27) Temmerman, K.; Nickel, W. A Novel Flow Cytometric Assay to Quantify Interactions between Proteins and Membrane Lipids. *J. Lipid Res.* **2009**, *50*, 1245–1254.
- (28) Liu, X.; Bing, T.; Shangguan, D. Microbead-Based Platform for Multiplex Detection of DNA and Protein. ACS Appl. Mater. Interfaces 2017, 9, 9462–9469.
- (29) Rivera, J. M.; Negrón, L. M. Supramolecular Hacky Sacks (SHS). *Method Synth. Applicat. Thereof.* **2018**, No. 10106572.
- (30) Honary, S.; Zahir, F. Effect of Zeta Potential on the Properties of Nano-Drug Delivery Systems A Review (Part 1). *Trop. J. Pharm. Res.* **2013**, *12*, 255–264.
- (31) Han, H.; Langley, D. R.; Rangan, A.; Hurley, L. H. Selective Interactions of Cationic Porphyrins with G-Quadruplex Structures. J. Am. Chem. Soc. 2001, 123, 8902–8913.
- (32) Murat, P.; Singh, Y.; Defrancq, E. Methods for Investigating G-Quadruplex DNA/Ligand Interactions. *Chem. Soc. Rev.* **2011**, *40*, 5293.
- (33) Vummidi, B. R.; Alzeer, J.; Luedtke, N. W. Fluorescent Probes for G-Quadruplex Structures. *Chem BioChem* **2013**, *14*, 540–558.
- (34) Adan, A.; Alizada, G.; Kiraz, Y.; Baran, Y.; Nalbant, A. Flow Cytometry: Basic Principles and Applications. *Crit. Rev. Biotechnol.* **2017**, *37*, 163–176.
- (35) Scolaro, L. M.; Castriciano, M.; Romeo, A.; Patanè, S.; Cefall, E.; Allegrini, M. Aggregation Behavior of Protoporphyrin IX in Aqueous Solutions: Clear Evidence of Vesicle Formation. *J. Phys. Chem. B* **2002**, *106*, 2453–2459.
- (36) Monchaud, D.; Allain, C.; Teulade-Fichou, M.-P. Thiazole Orange: A Useful Probe for Fluorescence Sensing of G-Quadruplex—Ligand Interactions. *Nucleosides, Nucleotides Nucleic Acids* **200**7, 26, 1585—1588.
- (37) Bhasikuttan, A. C.; Mohanty, J.; Pal, H. Interaction of Malachite Green with Guanine-Rich Single-Stranded DNA: Preferential Binding to a G-Quadruplex. *Angew. Chem., Int. Ed.* **2007**, *46*, 9305–9307.
- (38) Peters, G. M.; Skala, L. P.; Davis, J. T. A Molecular Chaperone for G4-Quartet Hydrogels. J. Am. Chem. Soc. 2016, 138, 134-139.

- (39) Acosta-Santiago, M. Biologically Relevant Formulation and Expansion of Responsive Properties of Guanine Based Supramolecular Particles; Ph.D., Universidad de Puerto Rico, San Juan, P.R., 2021.
- (40) Wei, C.; Jia, G.; Yuan, J.; Feng, Z.; Li, C. A Spectroscopic Study on the Interactions of Porphyrin with G-Quadruplex DNAs †. *Biochemistry* **2006**, *45*, 6681–6691.
- (41) Wheelhouse, R. T.; Sun, D.; Han, H.; Han, F. X.; Hurley, L. H. Cationic Porphyrins as Telomerase Inhibitors: The Interaction of Tetra-(*N*-Methyl-4-Pyridyl)Porphine with Quadruplex DNA. *J. Am. Chem. Soc.* **1998**, *120*, 3261–3262.
- (42) Parkinson, G. N.; Ghosh, R.; Neidle, S. Structural Basis for Binding of Porphyrin to Human Telomeres. *Biochemistry* **2007**, *46*, 2390–2397.
- (43) Danaei, M.; Kalantari, M.; Raji, M.; Samareh Fekri, H.; Saber, R.; Asnani, G. P.; Mortazavi, S. M.; Mozafari, M. R.; Rasti, B.; Taheriazam, A. Probing Nanoliposomes Using Single Particle Analytical Techniques: Effect of Excipients, Solvents, Phase Transition and Zeta Potential. *Heliyon* 2018, 4, e01088.